Three-Dimensional Spectral Radiative Heat Transfer Solutions by the Discrete-Ordinates Method

W. A. Fiveland* and A. S. Jamaluddin†
Babcock & Wilcox Company, Alliance, Ohio 44601

Radiative heat transfer in three-dimensional enclosures with a participating medium is predicted using the discrete-ordinates method formulated for spectral variations in the radiative properties. The spectral distribution of radiation is subdivided into a finite number of bands within which the properties are assumed uniform. The method uses a control volume formulation of the discrete-ordinates equations for each band. Solutions are found for each band, and are summed to obtain the total contribution. The solution strategy and stability are discussed in the paper. Results have been obtained for the S_4 method, a 24-flux approximation. Solutions are benchmarked with several methods. Examples are presented for enclosures with spectral walls and with absorbing mixtures, and absorbing and scattering media, to show the importance of mixture albedo and refractive index on net wall heat flux. The favorable results indicate that the spectral discrete-ordinates method offers an alternative that is easily adaptable and usable in existing control volume transport codes.

Nomenclature

A = north-south areas, m^2
a_n = coefficients of a Legendre series
B = east-west areas, m^2
C = front-back areas, m^2
$e_{b\lambda}$ = Planck's blackbody function
G = incident energy, W/m^2
I = radiant intensity, W/(m^2 · Sr)
L = enclosure dimension, m
L_m = mean beam length, m
m = complex refractive index
$\boldsymbol{n}$ = unit normal
N = number of terms in summation
q = heat flux, W/m^2
$\boldsymbol{r}$ = position vector, m
S = source term, W/m^3
T = temperature, K
V_p = volume of pth control volume, m^3
w_m = weight function in a direction m
x = distance along x-coordinate, m
$\bar{x}$ = fractional distance, x/L_x
y = distance along y-coordinate, m
$\bar{y}$ = fractional distance, y/L_y
z = distance along z-coordinate, m
$\bar{z}$ = fractional distance, z/L_z
α = finite-difference weighting factor ($0.5 \le \alpha \le 1.0$)
β = extinction coefficient, $\sigma + \kappa$, m^{-1}
ε = surface emittance or emissivity
κ = absorption coefficient, m^{-1}
λ = wavelength, μm
μ, ξ, η = ordinates $\mu = \cos\theta$, $\xi = \sin\theta \sin\phi$, $\eta = \sin\theta \cos\phi$
η = waveband, cm^{-1}
$\boldsymbol{\Omega}$ = outgoing direction of radiation
Φ = phase function
ρ = surface reflectance or reflectivity
σ = scattering coefficient, m^{-1}
$\bar{\sigma}$ = Boltzmann's constant, 5.669×10^{-8} W/(m^2 · K^4)
Θ = angle between incoming and outgoing intensity
ω = albedo of scatter, σ/β
∇ = gradient vector
Δ = fractional value

Subscripts
b = blackbody
g = gas
m = outgoing ordinate direction
m' = incoming ordinate direction
N, S, E, W, F, B = node points around p
n, s, e, w, f, b = control volume faces surrounding node point p
p = control volume center
r = radiative

Superscripts
$'$ = (prime) incoming value
m' = incoming direction

Received Feb. 19, 1990; revision received June 4, 1990; accepted for publication June 5, 1990.

*Senior Research Engineer, Research and Development Division.
†Supervisor, Research and Development Division. Member AIAA.

Introduction

In many high-temperature devices, including combustion in boilers and furnaces, radiant heat transfer is the dominant mode of energy transfer. Accurate prediction of the thermal performance of these processes is strongly linked to the proper determination of the radiation heat transfer. An extensive survey of multidimensional radiation models has been reported elsewhere.[1,2] Existing methods[3–7] of solving multidimensional problems are based on radiatively gray property assumptions. This paper describes a spectral discrete-ordinates method applicable for absorption, scattering, and re-emission of radiant energy in two- and three-dimensional Cartesian geometries. The method is an efficient, accurate, and stable computational tool for the analysis of radiative heat transfer.

Radiative properties are often very dependent on wavelength. Mixtures of absorbing gases, such as water vapor and carbon dioxide, and absorbing and scattering particles, like coal, char, and fly ash, need to be evaluated on a spectral basis. In this paper, the spectral absorption and emission characteristics of the medium are subdivided into a finite number of wavebands, within which the properties are constant. The discrete-ordinates equations for two- or three-dimensional geometries are derived. The picket fence method is used,[2] where each band is solved separately and total surface fluxes

and incident energy are found by adding the contributions of the individual bands. The theoretical treatment is presented, and a criterion for stability is given. The paper presents several examples to demonstrate the method and benchmark it against the numerically exact zone method. Predictions indicate that the spectral formulation is a good alternative for performing spectral radiative calculations.

Analysis

Consider the radiative transfer equation for the enclosure shown in Fig. 1. The balance of monochromatic energy passing in a specified direction Ω through a differential volume in an emitting-absorbing and scattering medium can be written as follows:

$$(\Omega \cdot \nabla)I(r, \Omega) = -(\kappa + \sigma)I(r, \Omega) + \kappa I_b(r) + \frac{\sigma}{4\pi}\int_{\Omega'=4\pi} I(r, \Omega')\,\Phi(\Omega' \to \Omega)\,d\Omega' \quad (1)$$

where $\Phi(\Omega' \to \Omega)$ is the phase function of energy transfer from the incoming direction Ω' to the outgoing direction Ω (see Fig. 1); $I(r, \Omega)$ is the radiation intensity, which is a function of position and direction; $I_b(r)$ is the intensity of a blackbody radiation at the temperature of the medium; and κ and σ are the absorption and scattering coefficients of the medium, respectively. The expression on the left-hand side represents the gradient of the intensity in the specified direction Ω. The three terms on the right represent the changes in intensity due to absorption and out-scattering, emission and in-scattering, respectively.

If the surface bounding the medium emits and reflects radiant energy, the radiative boundary condition for Eq. (1) is given by

$$I(r, \Omega) = \varepsilon I_b(r) + \frac{\rho}{\pi}\int_{n\cdot\Omega'<0} |n \cdot \Omega| I(r, \Omega')d\Omega' \quad (2)$$

where $I(r, \Omega)$ is the intensity of radiant energy leaving a surface at a boundary location, ε and ρ are the diffuse surface emissivity and surface reflectivity, respectively, and n is the unit normal vector at the boundary location.

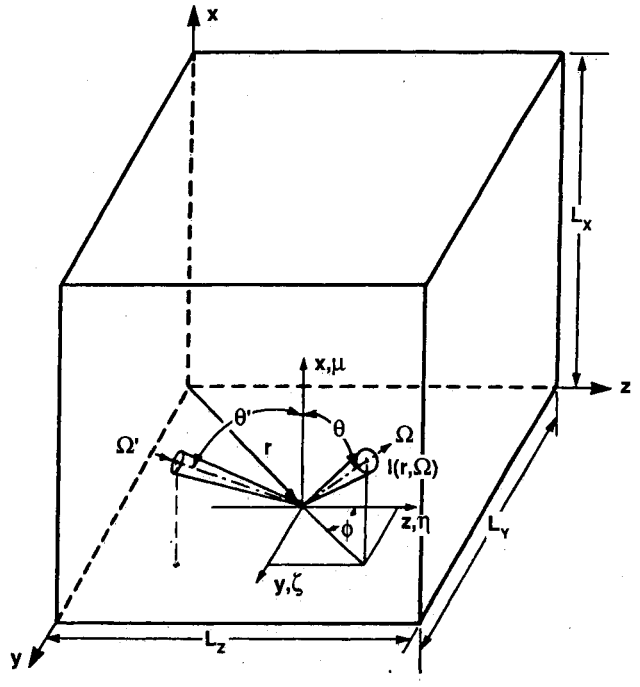

Fig. 1 Coordinate system.

Real systems exhibit a distribution of radiant energy that is nonuniform. Surface conditions in glass furnaces and combustors are typically nongray. Mixtures of absorbing gases and absorbing and scattering particles need to be evaluated on a spectral basis. However, practical considerations prohibit a wavelength-by-wavelength analysis. In this paper, the range of wavelengths is subdivided into a finite number of bands of width ($\Delta\lambda$) within which the radiation properties are assumed constant (radiatively gray). Eqs. (1) and (2) are written for each band, and calculations are performed. Once the band calculations are complete, the total net heat flux is calculated.

The radiative transfer equation for each band is approximated using the discrete-ordinates method.[6,7] For the multidimensional case, the transfer equation is also solved for a number of ordinate directions, and the integrals are replaced by a quadrature summed over the ordinate directions. For each band, the equation can be written:

$$\mu_m \frac{\partial I^m}{\partial x} + \xi_m \frac{\partial I^m}{\partial y} + \eta_m \frac{\partial I^m}{\partial z} = -\beta I^m + \kappa I_b + \frac{\sigma}{4\pi} S_m \quad (3)$$

For a discrete direction Ω_m, the values μ_m, ξ_m, and η_m are the direction cosines. The parameters β, κ, and σ represent, respectively, the band extinction, absorption, and scattering coefficients. And S_m is the source term for incoming radiation

$$S_m = \sum_{m'=1}^{Nm'} w_{m'}\,\Phi(m', m)I^{m'} \quad (4)$$

where

$$\Phi(m', m) = \sum_{n=0}^{N} (2n + 1)a_n P_n(\mu_m\mu_{m'} + \xi_m\xi_{m'} + \eta_m\eta_{m'}) \quad (5)$$

and the a_n represent Legendre coefficients for the phase function in each wave band.

The finite-difference approximation for each waveband is as follows [see Eqs. (23) in Ref. 6]:

$$I_p^m = \frac{\mu_m A I_w^m + \xi_m B I_s^m + \eta_m C I_b + \alpha(S_1 + S_2)V_p}{\mu_m A + \xi_m B + \eta_m C + \alpha\beta V_p} \quad (6)$$

where

$$A = \Delta y \Delta z$$
$$B = \Delta x \Delta z$$
$$C = \Delta x \Delta y$$
$$S_1 = \kappa \Delta I_b$$
$$S_2 = \frac{\sigma}{4\pi}\sum_{m'}^{Nm'} w_{m'}\Phi_{m'm}I_p^{m'}$$

The fact intensities are related to the cell center intensities as follows:

$$I_p^m = \alpha I_n^m + (1 - \alpha)I_s^m \quad (7)$$

$$I_p^m = \alpha I_e^m + (1 - \alpha)I_w^m \quad (8)$$

$$I_p^m = \alpha I_f^m + (1 - \alpha)I_b^m \quad (9)$$

The parameter α varies between 0.5 and 1. If $\alpha = 0.5$, Eqs. (7–9) represent the second-order diamond difference scheme proposed by Carlson and Lathrop[8] and, if $\alpha = 1.0$, a first-order difference method results. The solution of Eq. (6) follows the same procedure used before,[6] with the ordinates

listed there. The fractional energy emitted in each band is written as

$$\Delta I_b = \Delta F \frac{\bar{\sigma} T^4}{\pi} \tag{10}$$

where the quantity ΔF is

$$\Delta F = F(0 \rightarrow \lambda_2 T) - F(0 \rightarrow \lambda_1 T) \tag{11}$$

and

$$F(0 \rightarrow \lambda_1 T) \equiv \frac{\int_0^{\lambda_1} e_{b\lambda} d\lambda}{\int_0^{\infty} e_{b\lambda} d\lambda} \tag{12}$$

Chang and Rhee[9] have presented a function for the fractional emission in each waveband:

$$F(0 \rightarrow \lambda T) = \frac{15}{\pi^4} \sum_{n=1}^{\infty} \frac{e^{-nv}}{n} \left(v^3 + \frac{3v^2}{n} + \frac{6v}{n^2} + \frac{6}{n^3} \right) \tag{13}$$

where $v \equiv C_2/\lambda T$ and $C_2 = 14388$ μm K.

The total radiant flux from a surface is the sum of the net fluxes computed for each band:

$$q_{\text{net}} = \sum_{k=1}^{N_B} \pi \left[\varepsilon_k \Delta I_{b,k}(\boldsymbol{r}) - \frac{\varepsilon_k}{\pi} \sum_{m'=1}^{N_{m'}} w_{m'} \mu_{m'} I_k^{m'} \right] \tag{14}$$

The total incident energy to a control volume is the sum of the incident energies in each of the bands:

$$G = \sum_{k=1}^{N_B} \sum_{m=1}^{N_m} w_m I_k^m \tag{15}$$

Solution Stability

When Eq. (6) is used with Eqs. (7–9) to predict face intensity, the extrapolated face intensity may be negative, which is physically unrealistic. For each band, the conditions to maintain positive intensities are[6]:

$$\Delta x \leq \frac{|\mu|}{\beta(1-\alpha)} \phi, \qquad \Delta y \leq \frac{|\xi|}{\beta(1-\alpha)} \phi,$$

$$\Delta z \leq \frac{|\eta|}{\beta(1-\alpha)} \phi \tag{16}$$

where

$$\phi = \frac{\alpha^3 + (1-\alpha)^2(2-5\alpha)}{\alpha}$$

The algorithm for each waveband is similar and is started with $\alpha = 0.5$. If negative intensities are encountered as band-by-band calculations proceed, the band calculation is repeated with the value of α increased by 10%, until only positive intensities are computed or $\alpha = 1.0$ is reached. The first-order accurate method ($\alpha = 1$) guarantees positive intensities and, therefore, is stable regardless of the ordinate set or local radiative properties.

Results

This paper focuses on presentation of S_4 solutions, a 24-flux approximation, which was shown to be computationally efficient for the amount of numerical overhead.[6,7] All solutions were judged converged, based on a preset error of 0.01% in the incident energy.

Case 1

A unit cubical enclosure studied by Fiveland[6] was used to demonstrate that the spectral method with a number of bands, all having the same properties, reproduces the gray calculation. The walls of the enclosure were considered radiatively black ($\varepsilon = 1$), with unit emissive powers on the planes at $\bar{x} = 1$, $\bar{y} = 0$, and $\bar{z} = 0$ (emitting walls), and zero emissive powers on the receiving walls ($\bar{x} = 0$, $\bar{y} = 1$, and $\bar{z} = 1$). The medium was assumed in radiative equilibrium ($\nabla \cdot q = 0$). The total incident energy in a computational cell was found from a summation of the band incident energies, using Eq. (15). Temperature was determined from the relation

$$-\nabla \cdot q = \kappa(G - 4\sigma T^4) \tag{17}$$

Solutions were found with an extinction coefficient of $\kappa = 1.0$ m^{-1} and a computational grid of 125 control volumes (5 × 5 × 5). The surface heat flux for the gray and spectral discrete-ordinates solutions coincided, showing that the numerical scheme was coded properly.

Case 2

Edwards and Nelson[10] and Seigel and Howell[11] predicted radiative transfer between parallel nongray plates spaced 25.4 mm (1″). The plates were made of tungsten, and maintained at temperatures of 1111 K (2000°R) and 556 K (1000°R), respectively. Pure CO_2 at 1.013 MPa (10 atm) pressure and 556 K (1000°R) was maintained between the plates. Using the tabulated data in Seigel and Howell,[11] the absorption coefficients used in the spectral calculations (see Table 1) were obtained from the equation

$$\kappa_g = -\frac{1}{L_m} \ln(1 - \varepsilon_g)$$

The one-dimensional geometry was modeled using the 3-D model with a ratio of $L_y:L_x$ and $L_y:L_z$ of 1:24 and with a 4 × 4 × 4 computational grid. Under the assumed conditions, nearly 100% of energy leaving the 1111 K plate was received by the 556 K plate. The four end walls are modeled as reflecting surfaces, with an emittance approaching zero ($\varepsilon = 0.0001$).

The predicted local and average heat fluxes at the receiving surface are shown in Fig. 2. The fluxes obtained from the network method used by Edwards and Nelson and the exact solution presented by Seigel and Howell are also shown in the figure. Table 2 shows the numerical values of the average fluxes.

Most of the radiative transfer is in the transparent regions between the CO_2 absorption bands. In the bands $1141 \leq \eta \leq 2221$, $2430 \leq \eta \leq 3573$, and $3750 \leq \eta \leq \infty$, for example, the radiative transfer is 20.3%, 33.6%, and 42.6%, respectively, of the total. Only 3.5% of the radiative transfer occurs in the other bands.

The profiles of heat flux shown in Fig. 2 are not uniform, due to the end effects caused by modeling the one-dimensional geometry as three-dimensional. The variation in heat flux

Table 1 Spectral data for case 2

η band, cm^{-1}	$\Delta\lambda$, μm	ε_w	κ_g, m^{-1}
$\infty \rightarrow 3750$	$0 \rightarrow 2.67$	0.73	0
$3750 \rightarrow 3573$	$2.67 \rightarrow 2.798$	0.69	∞
$3573 \rightarrow 2430$	$2.798 \rightarrow 4.115$	0.61	0
$2430 \rightarrow 2221$	$4.115 \rightarrow 4.502$	0.65	∞
$2221 \rightarrow 1141$	$4.502 \rightarrow 8.764$	0.45	0
$1141 \rightarrow 1013$	$8.764 \rightarrow 9.871$	0.46	1.743
$1013 \rightarrow 849$	$9.871 \rightarrow 11.78$	0.37	1.348
$849 \rightarrow 779$	$11.78 \rightarrow 12.83$	0.32	0
$779 \rightarrow 555$	$12.83 \rightarrow 18.01$	0.26	49.05
$555 \rightarrow 0$	$18.01 \rightarrow \infty$	0.37	0

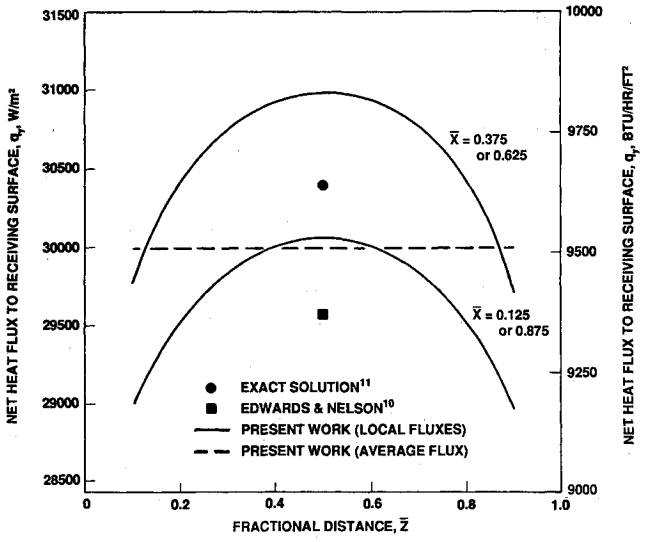

Fig. 2 Spectral heat flux to the receiving surface (case 2).

Table 2 Predicted average heat flux on the receiving surface

This study	29,991	w/m²
Edwards and Nelson (1962)	29,562	w/m²
Seigel and Howell (1972)	30,417	w/m²

(<3%, see Fig. 2) can be reduced by increasing L_x:L_y and L_z:L_y at the expense of additional computational time. As expected, the fluxes are somewhat higher for the two center rows of the grid.

Case 3

A cubical enclosure with side dimension 0.964 m ($\sqrt{10}$ ft) was modeled to compare the spectral discrete-ordinates and zone methods. The walls of the enclosure are maintained at a temperature of 1089 K (1960°R) and an emittance of ε = 0.6. The isothermal gas mixture at a temperature of 1367 K (2460°R) consists of 10% water vapor, 10% carbon dioxide, and 80% nitrogen by volume, maintained at a total pressure of 0.1013 MPa (1 atm).

The predicted radiant transfer between the gas and walls is shown in Fig. 3 for the discrete-ordinates and the zone methods.[12] Discrete-ordinates and zone calculations were performed using spectral properties obtained from wide-band models.[13] Surface and gas properties used in the analyses are shown in Table 3. A 5 × 5 × 5 computational grid was used in the calculations.

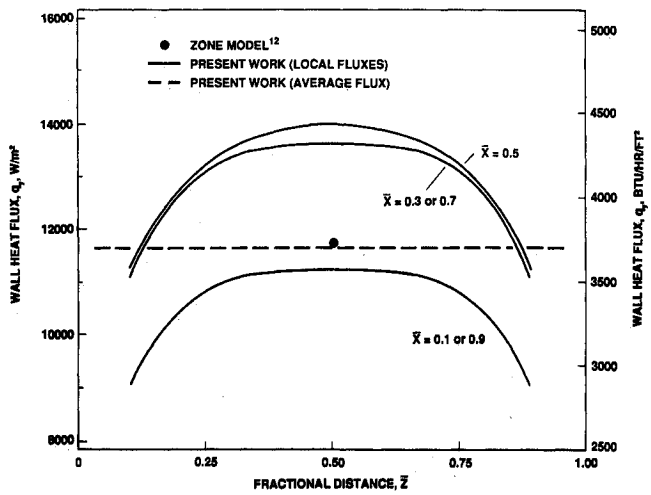

Fig. 3 Spectral heat flux on the walls (case 3).

Table 3 Spectral data for case 3

Wavelength, μm		Gas	Surface	Absorption
Min	Max	transmissivity	emissivity	coefficient, m^{-1}
0.100	1.357	1.0000	0.600	0.0003
1.357	1.402	0.9000	0.600	0.1873
1.402	1.812	1.0000	0.600	0.0003
1.812	1.918	0.9000	0.600	0.1873
1.918	1.928	0.8100	0.600	0.3747
1.928	1.930	0.9000	0.600	0.1873
1.930	2.429	1.0000	0.600	0.0003
2.429	2.574	0.7278	0.600	0.5650
2.574	2.911	0.5368	0.600	1.1063
2.911	2.938	0.7278	0.600	0.5650
2.938	4.149	1.0000	0.600	0.0003
4.149	4.654	0.1972	0.600	2.8871
4.654	5.425	1.0000	0.600	0.0003
5.425	7.372	0.5937	0.600	0.9272
7.372	9.299	1.0000	0.600	0.0003
9.299	9.572	0.9000	0.600	0.1873
9.572	10.254	1.0000	0.600	0.0003
10.254	10.585	0.9000	0.600	0.1873
10.585	12.514	1.0000	0.600	0.0003
12.514	12.886	0.2640	0.600	2.3681
12.886	17.922	0.0829	0.600	4.4281
17.922	24.390	0.2640	0.600	2.3681

The predicted average heat flux q_y at the wall is within 0.7% for either method. The curved profiles shown in the discrete-ordinates solution are caused by corner effects. Identical results were obtained for the average heat fluxes q_x and q_z.

A 10 × 10 × 10 grid was also used with similar results (the average heat flux agreed to within 0.1%). Substantially longer computer time (190.6 s as compared to 28.9 s for 5 × 5 × 5 grids on a SUN 4.0/260 workstation) was required for the larger grid.

Case 4

Calculations were performed for the enclosure described in case 3, using a 5 × 5 × 5 computational grid for several examples: gray walls and gray gas; gray walls and spectral gas; spectral walls and gray gas; and spectral walls and spectral gas. The measured normal spectral wall emittance[14] shown in Fig. 4 was used to model the spectral walls. The corresponding gray-wall emittance was 0.681. The gas mixture in case 3 (Table 3) was used to model the spectral gases, and a gray gas emissivity of 0.14 was used in the gray calculations.

Figure 5 exhibits the predicted wall heat flux, q_y vs $\bar{z}$ at $\bar{x}$ = 0.5, for the examples. For this application, the figure shows that the gas properties significantly affect the wall heat flux; the top two curves are the predicted heat flux profiles for the gray gas and the lower curves are the predicted profiles for the spectral gas. There is more than a 30% reduction in pre-

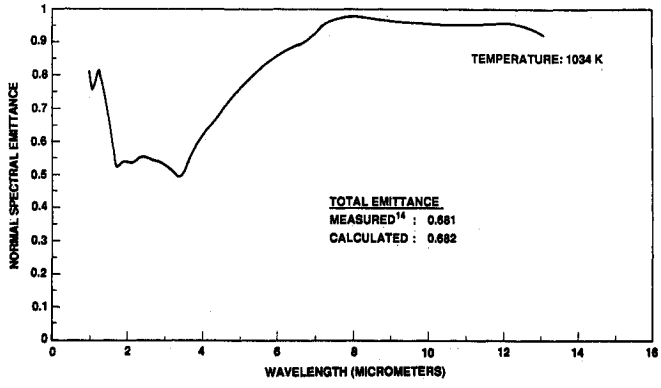

Fig. 4 Spectral emittance of a refractory material (DeBellis et al., 1989).

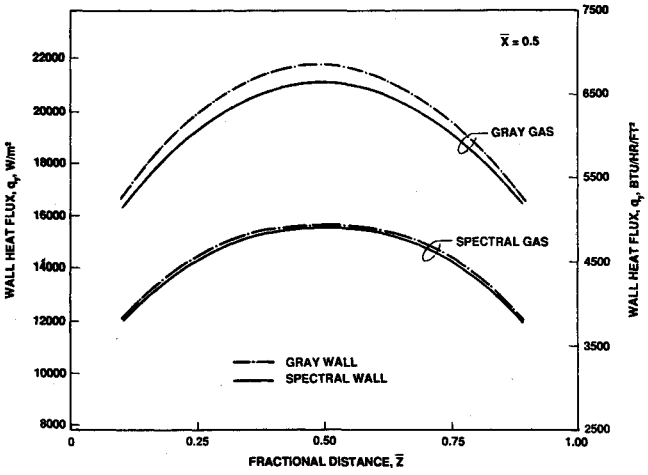

Fig. 5 Effect of spectral calculations on the predicted wall heat flux (case 4).

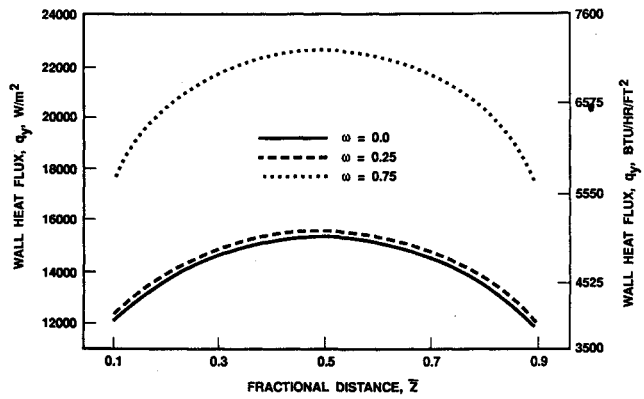

Fig. 6 Effect of scattering albedo on the predicted wall heat flux.

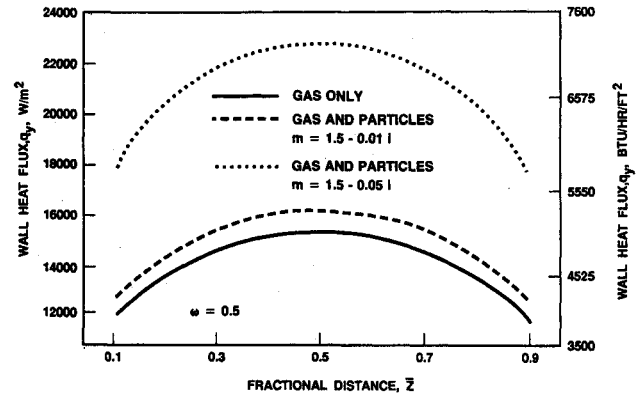

Fig. 7 Effect of complex refractive index of the particles on the predicted heat flux.

dicted heat flux for the examples with spectral gas. The wall emittance has a lesser effect; wall heat flux is reduced less than 4% when calculations simulate spectral walls instead of gray walls.

Case 5

An absorbing and scattering medium is considered in this case for the enclosure studied in cases 3 and 4. Absorption coefficients for the gas mixture are listed in Table 3. Particle absorption and scattering coefficients were found from Mie theory[15] for ash particles with a 15 μm size and a refractive index of 1.5–0.01i. Isotropic scattering was assumed. Spectral emittances shown in Fig. 4 were used to model the wall properties. Wall and mixture temperatures were the same as in cases 3 and 4.

Figure 6 shows the effect of scattering albedo, with the albedo varying between 0.0 and 0.75. The albedo was increased by the addition of particles into the initial gas mixture. The net wall heat flux increases as the albedo increases, since the source from volumetric emission and in-scattering effect an increased incident heat flux to the walls.

In Fig. 7, the effect on the predicted heat flux is shown for particle gas mixtures with varying refractive index of the ash particles. Three mixtures are considered: a gas mixture alone with the properties listed in Table 3, a particle-gas mixture with particles having a refractive index of 1.5–0.01i, and a particle-gas mixture with particles having a refractive index of 1.5–0.05i. A scattering albedo of 0.5 was assigned to the particle-gas mixture. The net wall flux increased, due to an increase in the volumetric source, which caused an increase in the incident and net wall heat flux.

Conclusions

A spectral discrete-ordinates method was formulated to demonstrate the importance of spectral calculations in nongray applications. The discrete-ordinates method is shown to be accurate in performing spectral radiation calculations. The calculations emphasize the need to collect spectral property data in furnaces, and show that consideration for nongray radiation may substantially improve furnace heat transfer predictions.

Acknowledgment

The authors want to thank the Gas Research Institute (GRI) for permitting use of the spectral emittance results shown in Fig. 4. These were collected under GRI Contract No. 5087-232-1579.

References

[1]Viskanta, R., "Radiative Heat Transfer," *Fortschritte der Verfahrenstechnik*, Vol. 22, 1984, pp. 51–81.

[2]Viskanta, R., and Menguc, M., "Radiation Heat Transfer in Combustion Systems," *Progress in Energy and Combustion Science*, Vol. 13, 1987, pp. 97–160.

[3]Howell, J. R., "Application of Monte Carlo to Heat Transfer Problems," *Advances in Heat Transfer*, Vol. 5, edited by T. F. Irvine, Jr., and J. P. Hartnett, Academic, NY, 1968, pp. 1–54.

[4]Lockwood, F. C., and Shah, N. G., "New Radiation Solution Method for Incorporation in General Combustion Prediction Procedures," *Proceedings of Eighteenth Symposium (International) on Combustion*, The Combustion Inst., Pittsburgh, PA, 1981, pp. 1405–1414.

[5]Menguc, M., and Viskanta, R., "Radiative Transfer in Three-Dimensional Rectangular Enclosures," *Journal of Quantum Spectroscopy and Radiative Transfer*, Vol. 33, 1985, pp. 533–549.

[6]Fiveland, W. A., *Journal of Thermophysics and Heat Transfer*, Vol. 2, No. 4, 1988, pp. 309–316.

[7]Jamaluddin, A. S., and Smith, P. J., "Predicting Radiative Transfer in Rectangular Enclosures Using the Discrete Ordinates Method," *Combustion Science and Technology*, Vol. 59, 1988, pp. 321–340.

[8]Carlson, B. G., and Lathrop, K. D., *Transport Theory—The Method of Discrete Ordinates in Computing Methods in Reactor Physics*, edited by Greenspan, Kelber, and Okrent, Gordon and Breach, NY, 1968.

[9]Chang, S. L., and Rhee, K. T., "Blackbody Radiation Functions," *International Comm. Heat Mass Transfer*, Vol. 11, 1984, pp. 451–455.

[10]Edwards, D., and Nelson, K., "Rapid Calculation of Radiant Energy Transfer Between Nongray Walls and Isothermal H_2O and CO_2 Gas," *Journal of Heat Transfer*, Vol. 84, No. 4, 1962, pp. 273–278.

[11]Seigel, R., and Howell, J., *Thermal Radiation Heat Transfer*, McGraw-Hill, 1972, p. 586.

[12]Hottel, H., and Sarofim, P., *Radiative Transfer*, McGraw-Hill, 1967.

[13]Edwards, D. K., "Molecular Gas Band Radiation," *Advances in Heat Transfer*, Vol. 12, 1976, pp. 115–193.

[14]DeBellis, C. L., Fiveland, W. A., and Bailey, R. T., "Effect of Refractory Emittance in Industrial Furnaces," Annual Report, Gas Research Inst., Contract No. 5087-232-1579, Jan. 1989.

[15]Van De Hulst, H. C., *Light Scattering by Small Particles*, Wiley, NY, 1957.